Swelling-Induced Morphology Reconstruction in Block Copolymer Nanorods: Kinetics and Impact of Surface Tension During Solvent Evaporation

Yong Wang,[†,*] Ling Tong,[†] and Martin Steinhart[‡,*]

[†]State Key Laboratory of Materials-Oriented Chemical Engineering, College of Chemistry and Chemical Engineering, Nanjing University of Technology, Nanjing 210009, Jiangsu, P. R. China, and [‡]Institute for Chemistry, University of Osnabrück, Barbarastrasse 7, D-49069 Osnabrück, Germany

ABSTRACT Nanoscopic domain structures of BCP nanorods can be converted into well-defined mesopore systems by swelling the BCP minority component with a selective solvent at temperatures below the bulk glass transition temperature of the nonswelling matrix. The initial stage of this process involves rapid morphology reconstruction of the nonswelling majority domains to accommodate the increased volume of the swelling minority domains caused by rapid solvent uptake. Morphology reconstruction slows down once entropic restoring forces of the swelling chains impede further uptake of swelling agent. Upon evaporation of the swelling agent, mesopores form in place of the swollen domains as the swollen minority blocks undergo entropic relaxation while intermediate nonequilibrium morphologies in the BCP nanorods are fixated by the reconstructed majority component. The surface area of mesopores developing when swollen cylindrical minority domains collapse may be minimized by the growth of Rayleigh instabilities. Depending on swelling temperature, swelling agent, and BCP architecture, BCP nanorods with one or several cylindrical channels undulated or uniform in diameter running along their long axes, linear strings of spherical cavities, and continuous mesopore systems can be obtained.

KEYWORDS: block copolymers · nanorods · swelling · mesopores · Rayleigh instabilities

Block copolymers (BCPs) containing two or more immiscible blocks may self-assemble into ordered nanoscopic domain structures characterized by spherical, cylindrical, gyroidal, and lamellar morphologies with periods typically ranging from ~10 to ~100 nm.[1,2] Nanopore systems in asymmetric amphiphilic BCPs may be generated by selective swelling of the minority domains accompanied by plastic deformation of the nonswollen or slightly swollen majority domains at temperatures well below the bulk glass transition temperature of the latter.[3] Evaporation of the swelling agent results in the collapse of the swollen minority blocks driven by entropic relaxation while the majority domains fixate the reconstructed morphology. As a result, mesopores form in place of the swollen minority domains. In the case of thin-film configurations, selective swelling pushes the minority blocks to the film surface, while the rigid majority domains undergo morphological reconstruction. The collapse of the swollen minority blocks upon evaporation of the solvent results in the formation of regular arrays of pores or dimples.[4−16] Nykänen *et al*. employed swelling in BCP films to control the permeability of filters.[17] Photonic properties of thick lamellar BCP films could be tuned *via* swelling-induced changes in periodicity.[18] Swelling-induced morphology reconstruction has also been exploited to develop well-defined mesopore systems in BCP membranes having thicknesses one to several orders of magnitude larger than the BCP period. Nanocellular polymeric monoliths were obtained in this way using fluorinated BCPs and supercritical carbon dioxide,[19] whereas polymeric membranes with bicontinuous nanoporous morphology resulted from swelling polystyrene-*block*-poly(2-vinylpyridine) (PS-*b*-P2VP) with ethanol.[20]

Self-assembly of BCPs in the cylindrical nanopores of shape-defining hard templates, such as anodic aluminum oxide (AAO), yields nanorods exhibiting the nanoscopic domain structure of the BCPs as an additional structure level.[21−25] The preparation of BCP nanorods by infiltration of BCP into AAO is outlined in Scheme 1. Swelling-induced morphology reconstruction in released nanorods consisting of cylinder-forming PS-*b*-P2VP containing P2VP as

*Address correspondence to yongwang@njut.edu.cn, martin.steinhart@uos.de.

Received for review October 31, 2010 and accepted February 2, 2011.

Published online February 16, 2011
10.1021/nn1029444

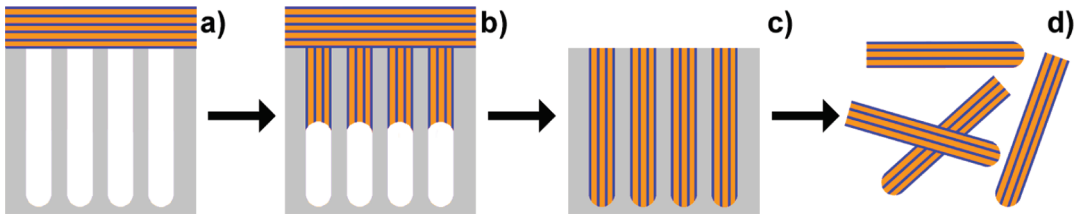

Scheme 1. Preparation of BCP nanorods by infiltration of an asymmetric BCP into AAO (orange, nonpolar majority component; blue, polar minority component; light grey, AAO). (a) The BCP is placed on top of AAO and heated to a temperature above the glass transition temperatures of its constituents. (b) The BCP infiltrates the AAO driven by capillarity. (c) After complete filling of the pores, residual BCP is removed from the surface of the AAO. (d) Suspensions of the BCP nanorods thus formed are obtained by etching the AAO. The domain structures at the menisci in panel b and the hemispherical nanorod tips in panels c and d are simplified—for details see ref 22.

swellable minority component and PS as nonswelling majority component at temperatures below the bulk glass transition temperature of PS (~100 °C) yielded mesoporous PS-*b*-P2VP nanorods.[26] It should be noted that this approach is different from that reported by Chen *et al*. involving the preparation of mesoporous polymer nanorods by swelling of solvent-annealed BCP nanotubes inside AAO at temperatures above the glass transition temperature of the nonswelling BCP component.[27] Mesoporous BCP nanorods obtained *via* swelling-induced morphology reconstruction have already been shown to template the synthesis of complex inorganic nanostructures[28] and should have considerable potential as nanoscopic building blocks with hierarchical architecture. However, predictive understanding of the kinetics of swelling-induced morphology reconstruction and of structure formation processes occurring during solvent evaporation is still at a premature stage.

The relatively high Flory–Huggins interaction parameter of PS and P2VP ($\chi = 91.6/T - 0.095$)[29] is indicative of strong driving forces for microphase separation in PS-*b*-P2VP, and polar solvents are expected to show high selectivity for P2VP. Therefore, we selected PS-*b*-P2VP nanorods containing either cylindrical or spherical P2VP domains to identify general kinetic patterns of swelling-induced morphology reconstruction and to elucidate to what extent additional structure formation processes during evaporation of the swelling agent influence mesopore formation.

RESULTS AND DISCUSSION

PS-*b*-P2VP Nanorods Containing Cylindrical P2VP Domains. Subjecting nanorods consisting of asymmetric PS-*b*-P2VP, which contain cylindrical domains of the minority component P2VP (Scheme 2, panel a), to swelling-induced morphology reconstruction yields polymeric nanorods having channels oriented along their long axes. Osmotic pressure drives the swelling agent ethanol, which is a good solvent for P2VP and a nonsolvent for PS,[30] into the cylindrical P2VP domains, which selectively swell. The pressure imposed by the swelling P2VP domains results in plastic deformation of the nonswollen PS matrix. At the initial stage of

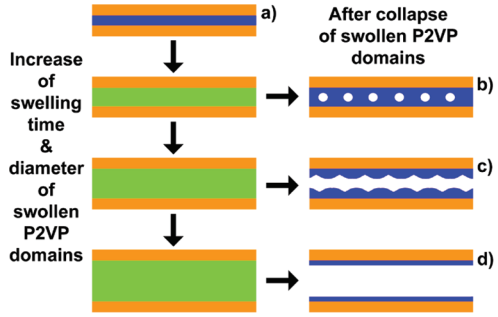

Scheme 2. Mesopore morphologies resulting from the collapse of swollen cylindrical P2VP domains after different swelling times. Orange, nonswollen PS matrix; light green, swollen P2VP; blue, nonswollen P2VP or collapsed P2VP after evaporation of the swelling agent.

morphology reconstruction, the diameter of the selectively swelling cylindrical P2VP domains and, therefore, the diameter of the cylindrical volume surrounded by the reconstructed PS matrix increases as more swelling agent migrates into the swelling domains. Morphology reconstruction is stopped by drying the PS-*b*-P2VP nanorods. The question arises whether structure formation processes occurring in the course of the collapse of the swollen P2VP blocks upon evaporation of the swelling agent affect the morphologies of the mesopores formed in place of the swollen P2VP domains.

The equilibrium state of liquids wetting the walls of cylindrical channels depends, in general, on the fraction of the channel volume occupied by the liquid. High filling ratios result in the development of strings of regularly arranged spherical cavities surrounded by the liquid *via* the growth of Rayleigh instabilities.[31,32] In the case of intermediate filling ratios, the surface area of liquid films wetting the wall of cylindrical channels may be minimized by the formation of periodic thickness undulations.[33] It is reasonable to assume that in the course of the evaporation of the swelling agent still-plasticized P2VP undergoes self-organization processes to develop morphologies representing the equilibrium state under the respective conditions as long as vitrification does not freeze structure evolution. At early stages of morphology reconstruction, even

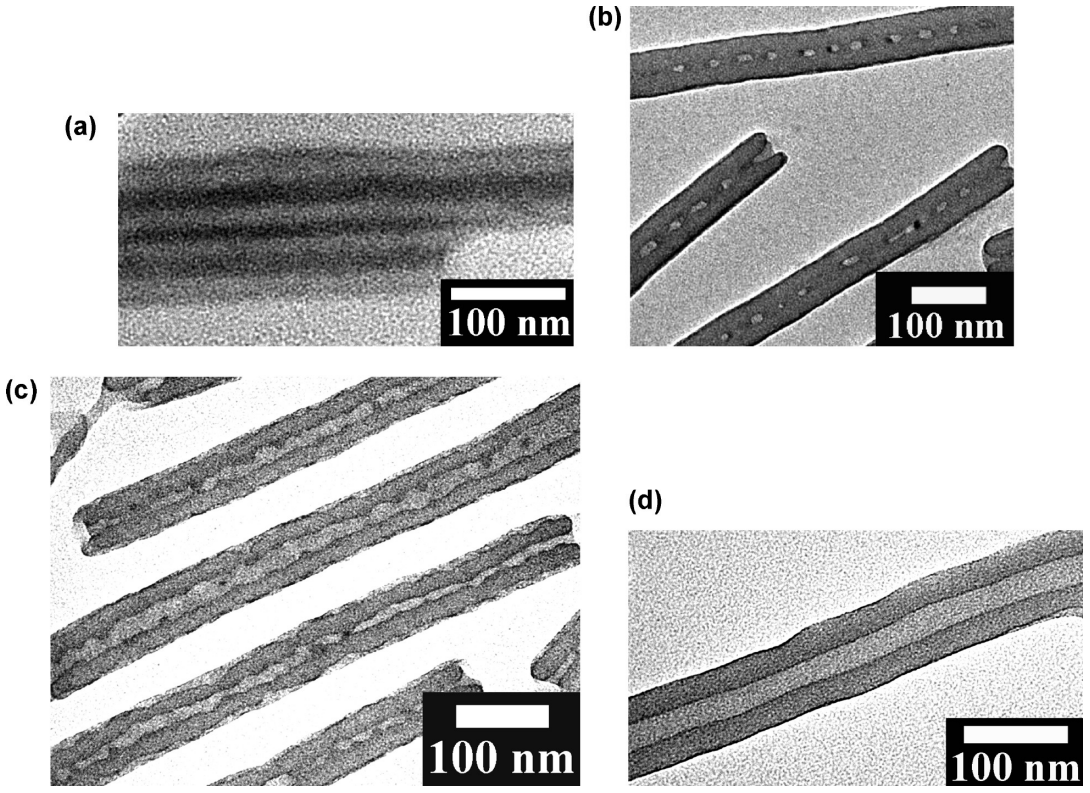

Figure 1. TEM images of (PS_18-*b*-P2VP_10)$_{60}$ nanorods released from AAO with a mean pore diameter of 60 nm. (a) Native (PS_18-*b*-P2VP_10)$_{60}$ nanorods. The P2VP domains are stained with iodine and appear dark. (b−d) Dried (PS_18-*b*-P2VP_10)$_{60}$ nanorods released from AAO with a mean pore diameter of 60 nm after exposure to ethanol for (b) 3 h at 20 °C, (c) 30 min at 40 °C, and (d) 66 h at 20 °C.

collapsed P2VP still occupies most of the cylindrical volume that accommodated the swollen cylindrical P2VP domains. Then, the internal surface area inside the PS-*b*-P2VP nanorods is apparently minimized by formation of discrete air cavities surrounded by P2VP reminiscent of morphologies resulting from the growth of Rayleigh instabilities[31] (Scheme 2, panel b). In such a configuration, at least some of the P2VP blocks must remain in a partially stretched state. Thus, minimization of the internal surface energy occurs at the expense of complete entropic relaxation of the P2VP blocks.

The diameter of the swollen P2VP domains and, therefore, that of the cylindrical space confined by the reconstructed rigid PS matrix increases in the course of the swelling process so that the volume fraction occupied by collapsed P2VP blocks in the absence of swelling agent becomes smaller. As a result, the collapsed P2VP blocks form undulated annular layers surrounding likewise undulated mesopores, (Scheme 2, panel c). Particularly in the case of fluids that cannot be transported over large distances, as in the case of the P2VP blocks, disconnected lobes were predicted to develop.[34] Surface undulations in the P2VP layers to minimize surface energy may develop on condition that the length scale at which the plasticized P2VP blocks connected to a rigid PS matrix can rearrange themselves matches the wavelength of the undulations. The wavelength of the undulations increases along with the diameter of the channels defined by the rigid reconstructed PS matrix in the course of swelling-induced morphology reconstruction. Hence, at later stages of morphology reconstruction the growth of undulations minimizing the internal surface area of the P2VP layer is suppressed because the P2VP blocks tethered to the PS matrix cannot rearrange themselves over distances corresponding to the wavelength of the undulations. Therefore, annular P2VP layers uniform in diameter surrounding straight cylindrical mesopores develop (Scheme 2, panel d). Thus, even if the channel geometry during swelling is consistently cylindrical, mesopores formed by the collapse of the P2VP chains are expected to be differently shaped after different swelling times.

Melt infiltration of PS_18-*b*-P2VP_10 (*Mn* (PS) = 17 500 g/mol; *Mn* (P2VP) = 9 500 g/mol, polydispersity = 1.10) into self-ordered AAO with a mean pore diameter of 60 nm[35] yielded (PS_18-*b*-P2VP_10)$_{60}$ nanorods (the subscript denotes the mean pore diameter of the AAO), which were released by etching the AAO. Selective staining of the P2VP domains with iodine[36] allows imaging the morphology of the (PS_18-*b*-P2VP_10)$_{60}$ nanorods by transmission

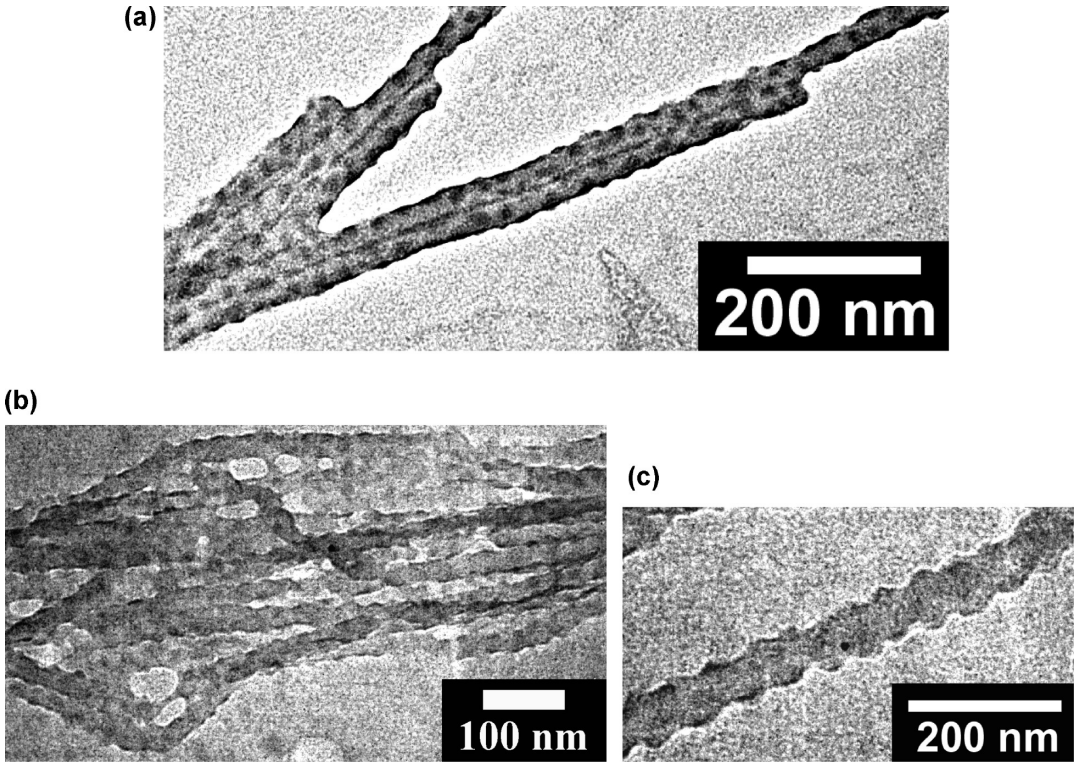

Figure 2. TEM images of (PS_50-*b*-P2VP_17)$_{25}$ nanorods released from AAO with a mean pore diameter of 25 nm. The P2VP domains were loaded with Na_2PtCl_4. (a) Overview of the spatial arrangement of the Pt-loaded P2VP domains (dark spots) on the outer surfaces of the (PS_50-*b*-P2VP_17)$_{25}$ nanorods; (b) undulated contour of (PS_50-*b*-P2VP_17)$_{25}$ nanorods; (c) view of the contour of a (PS_50-*b*-P2VP_17)$_{25}$ nanorod at higher magnification.

electron microscopy (TEM). They contain a cylindrical P2VP domain with an apparent diameter of about 20 nm appearing dark surrounded by a brighter PS matrix (Figure 1a). A thin continuous P2VP layer forms the outermost surface, as obvious from the presence of dark contrast lines at the edges of the (PS_18-*b*-P2VP_10)$_{60}$ nanorods. After swelling in ethanol for 3 h at 20 °C, dried (PS_18-*b*-P2VP_10)$_{60}$ nanorods indeed contained a string of spherical cavities with diameters of around 15 nm and a spacing of roughly 30 nm, corresponding to the morphology type displayed in panel b of Scheme 2. Dried (PS_18-*b*-P2VP_10)$_{60}$ nanorods swollen for 30 min in ethanol at 40 °C reached a more advanced stage of morphology reconstruction than their counterparts swollen for 3 h in ethanol at 20° C because of the strong temperature dependence of this process. Each (PS_18-*b*-P2VP_10)$_{60}$ nanorod swollen for 30 min in ethanol at 40 °C contains one continuous channel with a diameter of about 12 nm running along its long axis. However, periodic undulations of the channel diameter are clearly discernible (Figure 1c, corresponding to panel c in Scheme 2).

If the spherical cavities and channel undulations had developed during swelling-induced morphology reconstruction, these structural features would be imprinted into the PS matrix. Then, one would expect their further growth as swelling-induced morphology reconstruction proceeds, ultimately resulting in the development of multiple cleavages across the (PS_18-*b*-P2VP_10)$_{60}$ nanorods. However, the more morphology reconstruction proceeds, the more straight cylindrical channels are found as the dominating morphological feature, such as in the dried (PS_18-*b*-P2VP_10)$_{60}$ nanorod swollen in ethanol for 66 h at 20 °C seen in Figure 1d (corresponding to panel d in Scheme 2).

The development of surface undulations to minimize surface energy appears to be a generic feature of cylindrical films consisting of BCP blocks in the absence of hard confining walls. Figure 2 shows (PS_50-*b*-P2VP_17)$_{25}$ nanorods consisting of PS_50-*b*-P2VP_17 (M_n (PS) = 50000 g/mol; M_n (P2VP) = 16500 g/mol; polydispersity =1.09) released from AAO with a mean pore diameter of 25 nm.[37] The P2VP was stained with Na_2PtCl_4 and appears dark. The (PS_50-*b*-P2VP_17)$_{25}$ nanorods consist of a PS core, on the surface of which P2VP domains are seen as dark spots (Figure 2a). Similar to liquid films covering cylindrical fibers,[38] the outer P2VP layer exhibits periodic undulations with a wavelength of about 50 nm (Figure 2b,c).

(PS_50-*b*-P2VP_17)$_{180}$ nanorods[26] released from AAO with a mean pore diameter of 180 nm[39] contain several P2VP cylinders with a center-to-center distance of about 40 nm oriented parallel to the nanopore axes

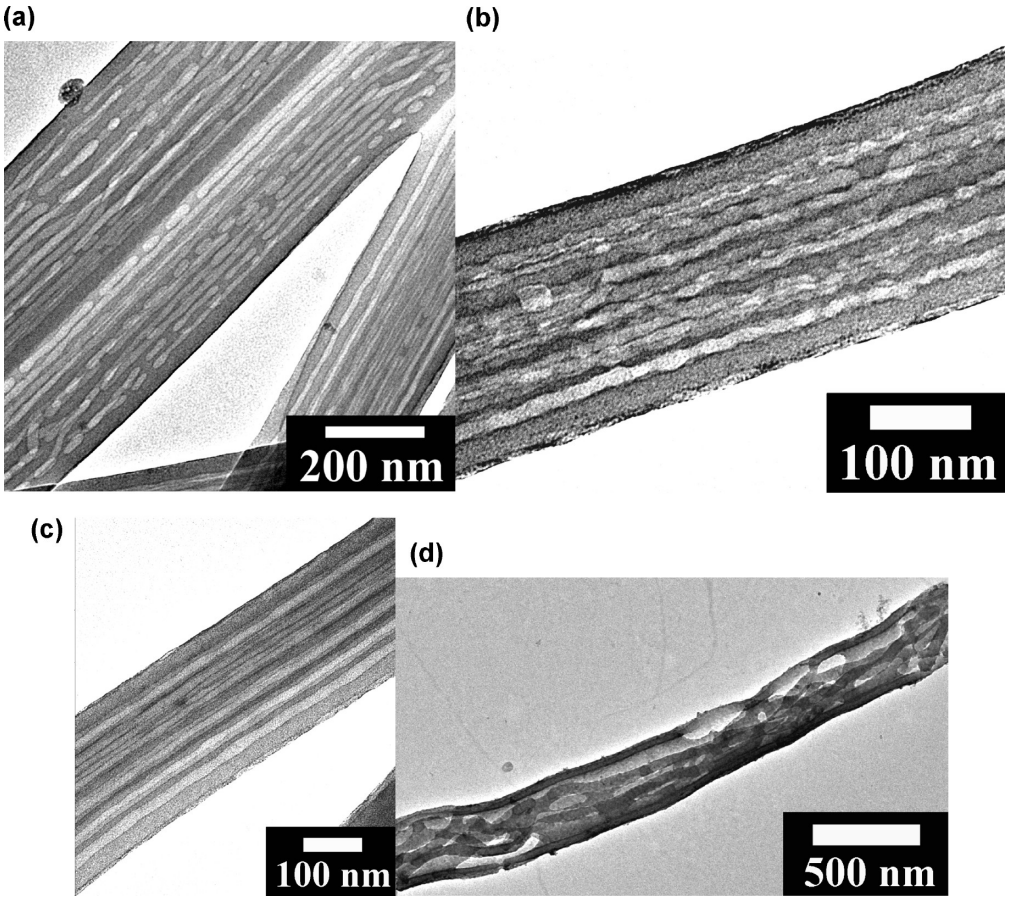

Figure 3. TEM images of dried (PS_50-*b*-P2VP_17)$_{180}$ nanorods released from AAO with a mean pore diameter of 180 nm after swelling in ethanol at 60 °C for (a) 10 min; (b), (c) 2 h. and (d) 72 h.

surrounded by a PS matrix, whereas their outermost surfaces consist of P2VP lamellae initially wetting the hydroxyl-terminated pore walls of the AAO (see ref 26 Figure 1, inset). Released (PS_50-*b*-P2VP_17)$_{180}$ nanorods were kept in ethanol for different periods of time at 60 °C. Regular strings of elongated plug-like cavities and nanochannels with a diameter of the order of 10 nm oriented parallel to the nanorod axes were apparent in dried (PS_50-*b*-P2VP_17)$_{180}$ nanorods after swelling in ethanol for 10 min at 60 °C (Figure 3a). After exposure to ethanol at 60 °C for 2 h, some dried (PS_50-*b*-P2VP_17)$_{180}$ nanorods contained continuous channels clearly exhibiting diameter undulations (Figure 3b), whereas other dried (PS_50-*b*-P2VP_17)$_{180}$ nanorods already contained cylindrical channels with a uniform diameter of about 20 nm (Figure 3c). Remarkably, distinct boundaries between the annular P2VP layers and the PS matrix are discernible, and the P2VP layer forming the outermost surface of the (PS_50-*b*-P2VP_17)$_{180}$ nanorods can clearly be identified. Further swelling in ethanol at 60 °C resulted in slow widening of now clearly cylindrical channels accompanied by gradual deterioration of the structural integrity of the nanorods. After swelling in ethanol for 72 h at 60 °C, dried (PS_50-*b*-P2VP_17)$_{180}$ nanorods contained isolated polymeric strands with apparent diameters of ~35 nm oriented along the nanorod axes surrounded by continuous outer shells. Hence, before drying an inverted morphology characterized by swollen P2VP matrices surrounding nonswollen PS domains existed. However, despite some defects, the outer polymeric shells still defined the surfaces of the (PS_50-*b*-P2VP_17)$_{180}$ nanorods (Figure 3d).

To access more advanced stages of swelling-induced morphology reconstruction, as displayed in Scheme 3, (PS_50-*b*-P2VP_17)$_{180}$ nanorods were treated with acetic acid, a good solvent for P2VP and a nonsolvent for PS.[30] Acetic acid (pK_a = 4.75) is less acidic than the cationic pyridinium groups of protonated P2VP (pK_a value ≈ 4.00)[40] so that protonation of the pyridyl moieties of the P2VP can be ruled out. However, already after swelling in acetic acid for 10 min at 20 °C, dried (PS_50-*b*-P2VP_17)$_{180}$ nanorods already contained cylindrical mesopores oriented parallel to their long axes with an apparent diameter of ~25 nm (Figure 4a), a stage of morphology reconstruction that corresponds to panel d in Scheme 2 and panel b in Scheme 3. After swelling in acetic acid for 10 min at 60 °C, dried (PS_50-*b*-P2VP_17)$_{180}$ nanorods consisted of bundles of partially interconnected cylindrical strands having diameters of ~45 nm (Figure 4b). While the spatial arrangement of the strands was still

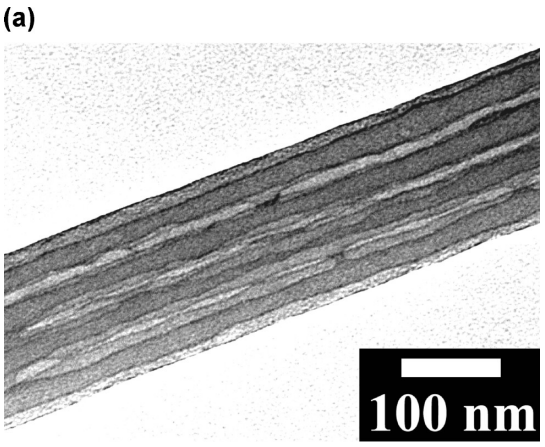

Figure 4. TEM images of dried (PS_50-*b*-P2VP_17)$_{180}$ nanorods released from AAO with a mean pore diameter of 180 nm after swelling in acetic acid for (a) 10 min at 20 °C, (b) 10 min at 60 °C, and (b) 17 h at 60 °C.

reminiscent of the initial nanorod topology, shells defining the surface of the (PS_50-*b*-P2VP_17)$_{180}$ nanorods no longer existed. Thus, swelling-induced reconstruction inverted the morphology of as-prepared (PS_50-*b*-P2VP_17)$_{180}$ nanorods characterized by cylindrical P2VP domains surrounded by a continuous PS matrix into a morphology characterized by PS strands surrounded by a swollen P2VP matrix, as visualized in panel c of Scheme 3. The drying of the thus-swollen (PS_50-*b*-P2VP_17)$_{180}$ nanorods yielded bundles of cylindrical strands with a PS core and a P2VP corona. Longer exposure to acetic acid at 60 °C led to slow conversion of the strands into spherical micelles that had an apparent diameter of ~65 nm in the dry state. The TEM image of a (PS_50-*b*-P2VP_17)$_{180}$ nanorod treated with acetic acid for 17 h at 60 °C seen in Figure 4c illustrates the gradual break-up of the cylindrical strands into spherical micelles. It should be noted that BCP micelles, as displayed in panel d of Scheme 3,

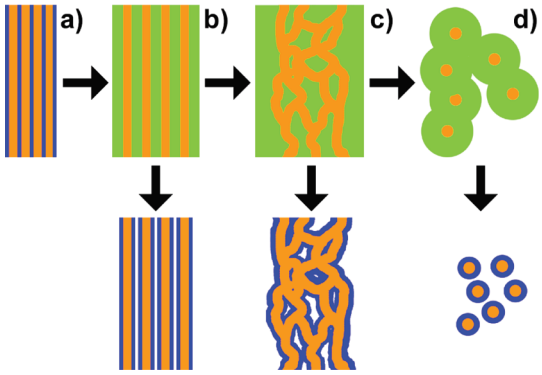

Scheme 3. Advanced stages of swelling-induced morphology reconstruction in PS-*b*-P2VP nanorods containing several cylindrical P2VP domains oriented parallel to the nanorod axis. Orange, nonswollen PS matrix; light green, swollen P2VP; blue, nonswollen P2VP and collapsed P2VP after evaporation of swelling agent. Panel b corresponds to panel d in Scheme 2.

are the equilibrium structures of amphiphilic BCPs in solvents selective for one block.[41,42]

PS-*b*-P2VP Nanorods Containing Spherical P2VP Domains. Figure 5a shows a native nanorod released from AAO with a mean pore diameter of 180 nm consisting of sphere-forming asymmetric PS_28-*b*-P2VP_4 (M_n (PS) = 27700 g/mol; M_n (P2VP) = 4300 g/mol, polydispersity = 1.04) with a bulk period of ~26 nm. The hemispherical tip of the (PS_28-*b*-P2VP_4)$_{180}$ nanorod is a replica of a likewise hemispherical pore bottom in the AAO hard template. Staining the P2VP with iodine revealed that the (PS_28-*b*-P2VP_4)$_{180}$ nanorods contain several rows of spherical P2VP domains appearing dark. After swelling in ethanol at 60 °C for 5 min, dried (PS_28-*b*-P2VP_4)$_{180}$ nanorods showed wormlike mesopore structures surrounded by a continuous, uniform cylindrical shell defining the nanorod surface (Figure 5b). The pressure imposed by neighboring rows of swelling P2VP spheres on the PS matrix caused rapid conversion of the sphere-in-matrix morphology into a bicontinuous structure consisting of interpenetrating networks of nonswollen PS domains and swollen P2VP domains. After swelling with ethanol for 10 min at 60 °C, dried (PS_28-*b*-P2VP_4)$_{180}$ nanorods consisted, therefore, of a continuous outer shell surrounding an apparently bicontinuous system of interconnected polymer strands with a diameter of ~20 nm and likewise interconnected mesopores with a diameter of ~20 nm (Figure 5c). In dried (PS_28-*b*-P2VP_4)$_{180}$ nanorods swollen at 60 °C for 2 h (Figure 5d) and even for 18 h (not shown) this morphology type was essentially retained. While the diameter of the polymer strands remained unaltered, the diameter of the mesopores slightly increased to about 25 nm after 2 h and to about 35 nm after 18 h. Moreover, the network of interconnected polymer strands in the interior of the (PS_28-*b*-P2VP_4)$_{180}$ nanorods completely detached from the outer shell.

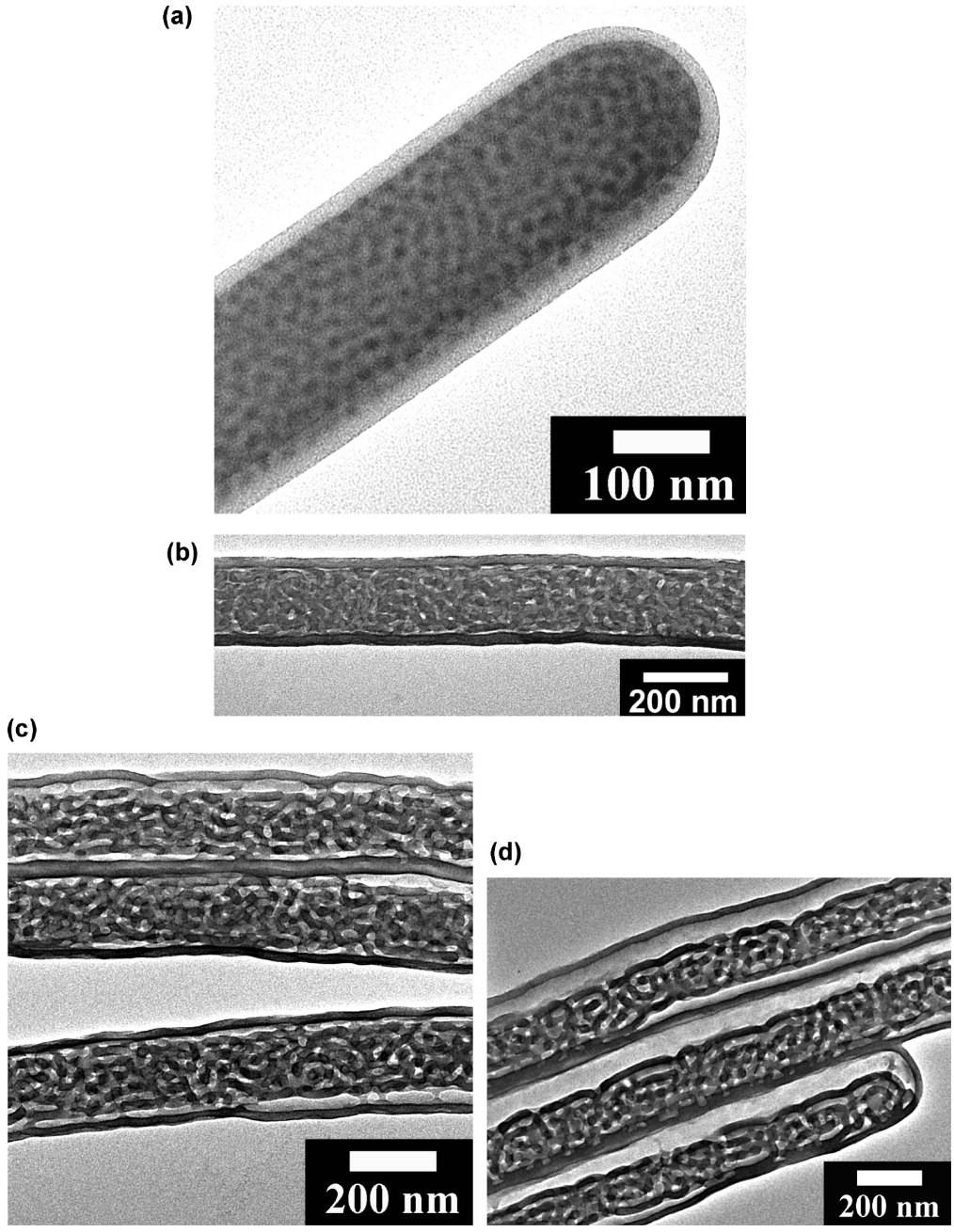

Figure 5. TEM images of (PS_28-*b*-P2VP_4)$_{180}$ nanorods released from AAO with a mean pore diameter of 180 nm. (a) Native (PS_28-*b*-P2VP_4)$_{180}$ nanorod. P2VP domains are stained with iodine and appear dark. (b−d) Dried (PS_28-*b*-P2VP_4)$_{180}$ nanorods after swelling in ethanol at 60 °C for (b) 5 min, (c) 10 min, and (d) 2 h.

A second shell had partially formed after 2 h and further developed as morphology reconstruction proceeded. Hence, slow interface-induced transformation of the network-like morphology rapidly formed during the initial swelling stage into a lamellar structure was apparent. However, the volume fraction of the P2VP domains attainable by swelling with ethanol at 60 °C was not large enough for an inversion of the morphology, which had resulted in the development of discrete PS entities surrounded by a swollen P2VP matrix as in the case of (PS_50-*b*-P2VP_17)$_{180}$ nanorods.

The question arises what happens if PS-*b*-P2VP nanorods contain only a single row of spherical P2VP domains. Staining the P2VP with iodine reveals that (PS_50-*b*-P2VP_17)$_{60}$ nanorods released from AAO with a mean pore diameter of 60 nm contain regular strings of spherical P2VP domains about 28 nm in diameter with a center-to-center distance of about 50 nm appearing dark surrounded by a brighter PS matrix (Figure 6a). The outer surface initially in contact with the hydroxyl-terminated pore walls of the AAO also consists of P2VP, as obvious from the dark contrast lines at the edges of the (PS_50-*b*-P2VP_17)$_{60}$

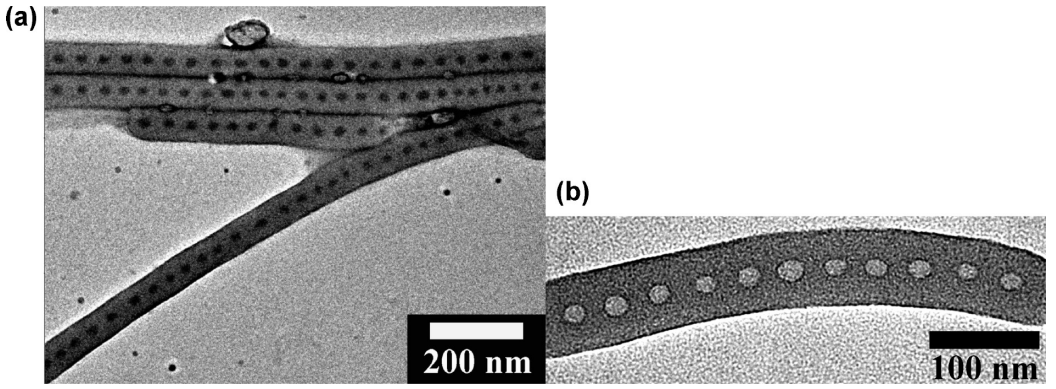

Figure 6. TEM images of (PS_50-*b*-P2VP_17)$_{60}$ nanorods released from AAO with a mean pore diameter of 60 nm. (a) Released native (PS_50-*b*-P2VP_17)$_{60}$ nanorods after etching the AAO. P2VP domains are stained with iodine and appear dark; (b) dried (PS_50-*b*-P2VP_17)$_{60}$ nanorod after exposure to ethanol for 18.5 h at 60 °C.

nanorods. After drying, (PS_50-*b*-P2VP_17)$_{60}$ nanorods swollen in ethanol for 18.5 h at 60 °C contained strings of hollow spheres ~23 nm in diameter, while their spacing of about 50 nm corresponded to that of native (PS_50-*b*-P2VP_17)$_{60}$ nanorods (Figure 6b). Contrary to the behavior of (PS_28-*b*-P2VP_4)$_{180}$ nanorods, the strings of spherical P2VP domains in the (PS_50-*b*-P2VP_17)$_{60}$ nanorods did not transform into bicontinuous or layered morphologies even after extended swelling times. Apparently, the PS matrix can adapt to the increased volume of the swollen P2VP spheres forming single rows since the outer P2VP layer at the surfaces of the (PS_50-*b*-P2VP_17)$_{60}$ nanorods can expand radially outward without restrictions. Hence, a morphology combining minimized internal surface area and complete entropic relaxation of the collapsed P2VP blocks can develop.

Kinetics of Swelling-Induced Morphology Reconstruction in BCP Nanorods. While some analogies between the swelling of rubbers[43] and swelling-induced morphology reconstruction in BCPs are straightforward, the former case commonly involves elastic deformation of a cross-linked network structure by solvent uptake. Morphology reconstruction in PS-*b*-P2VP nanorods by selective swelling the P2VP domains at temperatures below the bulk glass transition temperature of PS can be interpreted as a transformation from the equilibrium structure of PS-*b*-P2VP melt under cylindrical confinement into the micellar equilibrium structure of PS-*b*-P2VP dissolved in polar swelling agent. The initial stage of this process is characterized by rapid uptake of swelling agent accompanied by excluded volume expansion[44] of the swelling P2VP chains. Hence, pressure is exerted on the PS domains, which undergo plastic deformation while not at all or only slightly swollen. However, morphology reconstruction slows significantly down at intermediate stages of the structure transformation process. We speculate that, once a stage characterized by the maximum stretching of the swelling chains under the specific conditions applied is reached, further uptake of swelling agent is impeded. The limit for chain stretching is set by the balance of excluded-volume expansion and entropic restoring forces.[45] Driving forces for further structure transformation, such as reduction of the interfacial energy and further increase of the entropy of mixing, were apparently much weaker than those associated with the initial uptake of swelling agent.

Morphology reconstruction of (PS_50-*b*-P2VP_17)$_{180}$ nanorods in the course of swelling with ethanol at 60 °C (Figure 3) involved initial rapid widening of the swelling P2VP cylinders in the PS matrix. If acetic acid is used to swell (PS_50-*b*-P2VP_17)$_{180}$ nanorods at 60 °C (Figure 4), rapid morphology inversion resulting in the development of PS strands surrounded by a swollen P2VP matrix is observed. Both morphologies were obtained after swelling for only 10 min but persisted for several more hours under the same swelling conditions, before indications of a slowly ongoing structural transformation became apparent. At a stage characterized by swollen but still cylindrical P2VP domains in a continuous PS matrix morphology reconstruction in ethanol at 60 °C decelerates, and slow morphology inversion converting the swollen P2VP domains into a matrix surrounding nonswollen PS strands follows. In the course of the swelling of (PS_50-*b*-P2VP_17)$_{180}$ nanorods with acetic acid at 60 °C, morphology reconstruction decelerates once PS strands surrounded by a swollen P2VP matrix have been formed, which are then slowly transformed into spherical micelles. This outcome suggests that (PS_50-*b*-P2VP_17)$_{180}$ nanorods swollen either in ethanol or acetic acid under otherwise identical conditions reach significantly different morphological stages after the same swelling times. It should also be noted that structure evolution in (PS_28-*b*-P2VP_4)$_{180}$ nanorods swollen in ethanol at 60 °C (Figure 5) involves rapid initial conversion of a spheres-in-matrix morphology into a bicontinuous one, which then slowly transforms into a lamellar structure. The stage at which swelling-induced morphology reconstruction decelerates appears to depend largely on the enthalpic interactions

between swelling agent and swelling blocks as well as on the architecture of the BCP.

Changes in the Gibbs free energy G in the course of swelling-induced morphology reconstruction comprise contributions related to the mixing of swelling agent and swelling blocks, contributions related to chain stretching, as well as contributions related to the interfacial energy of the PS domains. The attainable minimum of G defines the equilibrium state and consequently the ultimate end point of swelling-induced morphology reconstruction at a given temperature. However, since G is commonly a function of temperature, significantly different equilibrium states may exist at different temperatures. It is, moreover, reasonable to assume that enthalpic interactions between swelling agent and swelling blocks, which depend on the selected swelling agent/BCP system and the swelling temperature, influence the position of the equilibrium state. We nevertheless speculate that the generation of specific mesopore systems in BCP nanorods can predominantly be achieved by kinetic control over the morphology transformation.

Differences to Swelling-Induced Morphology Reconstruction in Thin Films. The absence of hard confining interfaces distinguishes swelling-induced morphology reconstruction in suspended BCP nanorods from swelling-induced morphology reconstruction in thin BCP films supported by rigid inorganic substrates.[4−16] Polymer chains cannot penetrate rigid interfaces so that confinement impedes morphology reconstruction in BCP films deposited on rigid inorganic substrates by spin coating or similar techniques. Moreover, irreversible adsorption of blocks having high affinity to the inorganic substrates, for example, by formation of hydrogen bonds, and the limited range of accessible conformational states in the vicinity of the polymer/solid interface may impede dynamic processes. Hence, morphology reconstruction processes in thin-film configurations will most probably be located at the polymer/air interface, resulting in rapid piercing of encapsulated domains of the swelling minority component through the nonswelling matrix toward the polymer/air interface. However, since the thin BCP films as such are conserved owing to the presence of rigid inorganic substrates, morphology reconstruction can often be reversed by exposure of the reconstructed BCP films to solvents having selectivities opposite to those initially used as swelling agent.

CONCLUSIONS

Well-defined mesopore systems in BCP nanorods are accessible by selectively swelling spherical or cylindrical domains of the BCP minority component at temperatures below the bulk glass transition temperature of the nonswelling BCP majority component. The pressure the expanding minority domains exert on the nonswelling matrix of the majority component results in plastic deformation of the latter. At the initial stage of swelling-induced morphology reconstruction, rapid solvent uptake of the minority domains is accompanied by rapid plastic deformation of the nonswelling matrix. Morphology reconstruction significantly decelerates once entropic restoring forces of the swelling chains impede further uptake of swelling agent. Depending on swelling temperature, swelling agent, and BCP architecture various nonequilibrium morphologies can easily be conserved by evaporation of the swelling agent. The swollen minority blocks collapse upon evaporation of the swelling agent while the nonswollen matrix fixates the reconstructed morphology. Hence, mesopores form in place of the swollen minority domains. Collapsing cylindrical minority domains undergo additional self-organization processes during solvent evaporation to minimize the surface area of the developing mesopores. At early stages of morphology reconstruction corresponding to small diameters of the swollen domains, their collapse results in the development of strings of spherical cavities *via* the growth of Rayleigh instabilities. At more advanced stages characterized by larger diameters of the swollen domains, their collapse results in the formation of undulated annular layers. At even later stages, the collapsing blocks tethered to the nonswollen matrix cannot be transported over distances corresponding to the wavelength of the undulations, which increases along with the channel diameter, and form uniform layers. Thus, nanoscopic domain structures in BCP nanorods can be converted into strings of spherical cavities, single or multiple cylindrical mesopores uniform in diameter or undulated oriented parallel to the nanorod axes, bicontinuous mesopore systems surrounded by continuous outer shells, and interconnected bundles of micellar strands. Swelling-induced morphology reconstruction is not only applicable to BCP nanorods prepared by means of shape-defining hard templates, such as AAO, but also to electrospun BCP nanofibers.[46−48]

EXPERIMENTAL SECTION

Preparation of BCP Nanorods (See Also Scheme 1). All BCPs were obtained from Polymer Source Inc., Canada, and used as received. Self-ordered nanoporous AAO with a pore depth of 100 μm and mean pore diameters of 25,[37] 60,[35] and 180 nm[39] was prepared following procedures reported in the literature. BCPs located on top of self-ordered AAO were heated to 230 °C for 24 h while applying a load of approximately 0.7 kg/cm^2 to accelerate infiltration. The infiltrated AAO membranes were removed from the furnaces, and residual BCP on the surface of the AAO was removed with sharp blades. The AAO was etched with 40 wt % aqueous KOH solution for ~20 min at room temperature. Subsequently,

three washing steps involving centrifugation, removal of the supernatant solution, and redispersion in deionized water, another washing step with 40 wt % aqueous KOH solution, and three washing steps with deionized water, as described above, were performed. In the course of this procedure, PS-*b*-P2VP nanorods with diameters of 60 nm and below broke into sections with lengths ranging from 1 μm up to a few μm, and PS-*b*-P2VP nanorods with diameters of 180 nm and above broke into sections with lengths of about 10 μm. The released BCP nanorods were suspended in ethanol and stored at 20 °C. During storage under these conditions, swelling-induced morphology reconstruction did not occur to a significant extent, as revealed by TEM investigations.

Swelling-Induced Morphology Reconstruction in BCP Nanorods. Aliquots of the ethanolic nanorod suspensions were placed in cuvettes. The ethanol was allowed to evaporate for ~24 h. The precipitates thus obtained were redispersed in about 1 mL of swelling agent (ethanol or acetic acid, purchased from Fluka, purity >98%) preheated to the desired swelling temperature. After the selected swelling time, small amounts of the suspensions were deposited on carbon-coated copper grids for TEM investigations. Apart from some defects, the observed morphologies were usually uniform along both native nanorods and nanorods subjected to swelling-induced morphology reconstruction.

Characterization of the BCP Nanorods. As-released native (PS_18-*b*-P2VP_10)$_{60}$ nanorods, (PS_28-*b*-P2VP_4)$_{180}$ nanorods, and (PS_50-b-P2VP_17)$_{60}$ nanorods deposited onto carbon-coated copper grids were stained with iodine[36] in a sealed container heated to 60 °C for 30 min. Iodine selectively enriched in the P2VP domains, which appear darker than the PS domains in TEM images. The P2VP domains of (PS_50-*b*-P2VP_17)$_{25}$ nanorods were loaded with Na_2PtCl_4 in a solution of 1 wt % Na_2PtCl_4 in a 1:1 (v/v) water/ethanol mixture for 10 min, followed by washing in 1:1 (v/v) water/ethanol mixtures. TEM investigations were carried out on a JEOL 1010 microscope operated at 100 keV.

Acknowledgment. Support from the National Natural Science Foundation of China (Grant 21004033), the Jiangsu Natural Science Foundation (Grant BK2009358), the Open Research Fund Program of the State Key Laboratory of Polymer Physics and Chemistry (Changchun Institute of Applied Chemistry), and the German Research Foundation (Priority Program 1420) is gratefully acknowledged. We thank S. Kallaus and K. Sklarek for the preparation of AAO.

REFERENCES AND NOTES

1. Bates, F. S.; Fredrickson, G. H. Block Copolymer Thermodynamics—Theory and Experiment. *Annu. Rev. Phys. Chem.* **1990,** *41*, 525–557.
2. Abetz, V.; Simon, P. F. W. Phase Behaviour and Morphologies of Block Copolymers. *Adv. Polym. Sci.* **2005,** *189*, 125–212.
3. Nykänen, A.; Nuopponen, M.; Hiekkataipale, P.; Hirvonen, S.-P.; Soininen, A.; Tenhu, H.; Ikkala, O.; Mezzenga, R.; Ruokolainen, J. Direct Imaging of Nanoscopic Plastic Deformation Below Bulk T_g and Chain Stretching in Temperature-Responsive Block Copolymer Hydrogels by cryo-TEM. *Macromolecules* **2008,** *41*, 3243–3249.
4. Boontongkong, Y.; Cohen, R. E. Cavitated Block Copolymer Micellar Thin Films: Lateral Arrays of Open Nanoreactors. *Macromolecules* **2002,** *35*, 3647–3652.
5. Xu, T.; Stevens, J.; Villa, J. A.; Goldbach, J. T.; Guarim, K. W.; Black, C. T.; Hawker, C. J.; Russell, T. R. Block Copolymer Surface Reconstuction: A Reversible Route to Nanoporous Films. *Adv. Funct. Mater.* **2003,** *13*, 698–702.
6. Sidorenko, A.; Tokarev, I.; Minko, S.; Stamm, M. Ordered Reactive Nanomembranes/Nanotemplates from Thin Films of Block Copolymer Supramolecular Assembly. *J. Am. Chem. Soc.* **2003,** *125*, 12211–12216.
7. Cong, Y.; Zhang, Z. X.; Fu, J.; Li, J.; Han, Y. C. Water-Induced Morphology Evolution of Block Copolymer Micellar Thin Films. *Polymer* **2005,** *46*, 5377–5384.
8. Li, X.; Tian, S. J.; Ping, Y.; Kim, D. H.; Knoll, W. One-Step Route to the Fabrication of Highly Porous Polyaniline Nanofiber Films by Using PS-*b*-PVP Diblock Copolymers as Templates. *Langmuir* **2005,** *21*, 9393–9397.
9. Xu, C.; Fu, X. F.; Fryd, M.; Xu, S.; Wayland, B. B.; Winey, K. I.; Composto, R. J. Reversible Stimuli-Responsive Nanostructures Assembled from Amphiphilic Block Copolymers. *Nano Lett.* **2006,** *6*, 282–287.
10. Chai, J.; Wang, D.; Fan, X.; Buriak, J. M. Assembly of Aligned Linear Metallic Patterns on Silicon. *Nat. Nanotechnol.* **2007,** *2*, 500–506.
11. Miller, A. C.; Bennett, R. D.; Hammond, P. T.; Irvine, D. J.; Cohen, R. E. Functional Nanocavity Arrays *via* Amphiphilic Block Copolymer Thin Films. *Macromolecules* **2008,** *41*, 1739–1744.
12. Chai, J.; Buriak, J. M. Using Cylindrical Domains of Block Copolymers to Self-Assemble and Align Metallic Nanowires. *ACS Nano* **2008,** *2*, 489–501.
13. Wang, Y.; Liu, J. Q.; Christiansen, S.; Kim, D. H.; Gösele, U.; Steinhart, M. Nanopatterned Carbon Films with Engineered Morphology by Direct Carbonization of UV-Stabilized Block Copolymer Films. *Nano Lett.* **2008,** *8*, 3993–3997.
14. Wang, Y.; Becker, M.; Wang, L.; Liu, J.; Scholz, R.; Peng, J.; Gösele, U.; Christiansen, S. H.; Kim, D. H.; Steinhart, M. Nanostructured Gold Films for SERS by Block Copolymer-Templated Galvanic Displacement Reactions. *Nano Lett.* **2009,** *9*, 2384–2389.
15. Zhang, R.; Yokoyama, H. Fabrication of Nanoporous Structures in Block Copolymer Using Selective Solvent Assisted with Compressed Carbon Dioxide. *Macromolecules* **2009,** *42*, 3559–3564.
16. Park, J. H.; Sun, Y.; Goldman, Y. E.; Composto, R. J. Amphiphilic Block Copolymer Films: Phase Transition, Stabilization, and Nanoscale Templates. *Macromolecules* **2009,** *42*, 1017–1023.
17. Nykänen, A.; Nuopponen, M.; Laukkanen, A.; Hirvonen, S.-P.; Rytelal, M.; Turunen, O.; Tenhu, H.; Mezzenga, R.; Ikkala, O.; Ruokolainen, J. Phase Behavior and Temperature-Responsive Molecular Filters Based on Self-Assembly of Polystyrene-*block*-poly(*N*-isopropylacrylamide)-*block*-polystyrene. *Macromolecules* **2007,** *40*, 5827–5834.
18. Kang, Y.; Walish, J. J.; Gorishnyy, T.; Thomas, E. L. Broad-Wavelength-Range Chemically Tunable Block-Copolymer Photonic Gels. *Nat. Mater.* **2007,** *6*, 957–960.
19. Yokoyama, H.; Li, L.; Nemoto, T.; Sugiyama, K. Tunable Nanocellular Polymeric Monoliths Using Fluorinated Block Copolymer Templates and Supercritical Carbon Dioxide. *Adv. Mater.* **2004,** *16*, 1542–1545.
20. Wang, Y.; He, C.; Xing, W.; Li, F.; Tong, L.; Chen, Z.; Liao, X.; Steinhart, M. Nanoporous Metal Membranes with Bicontinuous Morphology from Recyclable Block Copolymer Templates. *Adv. Mater.* **2010,** *22*, 2068–2072.
21. Shin, K.; Xiang, H. Q.; Moon, S. I.; Kim, T.; McCarthy, T. J.; Russell, T. P. Curving and Frustrating Flatland. *Science* **2004,** *306*, 76.
22. Xiang, H. Q.; Shin, K.; Kim, T.; Moon, S. I.; McCarthy, T. J.; Russell, T. P. Block Copolymers Under Cylindrical Confinement. *Macromolecules* **2004,** *37*, 5660–5664.
23. Sun, Y. M.; Steinhart, M.; Zschech, D.; Adhikari, R.; Michler, G. H.; Gösele, U. Diameter-Dependence of the Morphology of PS-b-PMMA Nanorods Confined Within Ordered Porous Alumina Templates. *Macromol. Rapid Commun.* **2005,** *26*, 369–375.
24. Dobriyal, P.; Xiang, H.; Kazuyuki, M.; Chen, J.-T.; Jinnai, H.; Russell, T. P. Cylindrically Confined Diblock Copolymers. *Macromolecules* **2009,** *42*, 9082–9088.
25. Yu, B.; Sun, P.; Chen, T.; Jin, Q.; Ding, D.; Li, B. Confinement-Induced Novel Morphologies of Block Copolymers. *Phys. Rev. Lett.* **2006**, *96*, 138306 (1—4).
26. Wang, Y.; Gösele, U.; Steinhart, M. Mesoporous Block Copolymer Nanorods by Swelling-Induced Morphology Reconstruction. *Nano Lett.* **2008,** *8*, 3548–3553.
27. Chen, D.; Park, S.; Chen, J. T.; Redston, E.; Russell, T. P. A Simple Route for the Preparation of Mesoporous Nanostructures Using Block Copolymers. *ACS Nano* **2009,** *3*, 2827–2833.
28. Wang, Y.; Qin, Y.; Berger, A.; Yau, E.; He, C.; Zhang, L.; Gösele, U.; Knez, M.; Steinhart, M. Nanoscopic Morphologies in Block Copolymer Nanorods as Templates for

Atomic Layer Deposition of Semiconductors. *Adv. Mater.* **2009,** *21*, 2763–2766.
29. Schulz, M. F.; Khandpur, A. K.; Bates, F. S.; Almdal, K.; Mortensen, K.; Hajduk, D. A.; Gruner, S. M. Phase Behavior of Polystyrene-poly(2-vinylpyridine) Diblock Copolymers. *Macromolecules* **1996,** *29*, 2857–2867.
30. Brandrup, J., Immergut, E. H., Eds. *Polymer Handbook*, 3rd ed.; John Wiley & Sons: New York, 1989.
31. Lord Rayleigh. On the Instability of Cylindrical Fluid Surfaces. *Phil. Mag. Ser. 5* **1892**, *34*, 177-180.
32. Chen, J. T.; Zhang, M. F.; Russell, T. P. Instabilities in Nanoporous Media. *Nano Lett.* **2007,** *7*, 183–187.
33. Everett, D. H.; Haynes, J. M. Model Studies of Capillary Condensation. I. Cylindrical Pore Model with Zero Contact Angle. *J. Colloid Interface Sci.* **1972,** *38*, 125–137.
34. Hammond, P. S. Nonlinear Adjustment of a Thin Annular Film of Viscous Fluid Surrounding a Thread of Another Within a Circular Pipe. *J. Fluid Mech.* **1983,** *137*, 363–384.
35. Masuda, H.; Fukuda, K. Ordered Metal Nanohole Arrays Made by a Two-Step Replication of Honeycomb Structures of Anodic Alumina. *Science* **1995,** *268*, 1466–1468.
36. Chiu, J. J.; Kim, B. J.; Kramer, E. J.; Pine, D. J. Control of Nanoparticle Location in Block Copolymers. *J. Am. Chem. Soc.* **2005,** *127*, 5036.
37. Masuda, H.; Hasegawa, F.; Ono, S. Self-Ordering of Cell Arrangement of Anodic Porous Alumina Formed in Sulphuric Acid Solution. *J. Electrochem. Soc.* **1997,** *144*, L127–L130.
38. Quéré, D.; Di Meglio, J.-M.; Brochard-Wyart, F. Spreading of Liquids on Highly Curved Surfaces. *Science* **1990,** *249*, 1256–1260.
39. Masuda, H.; Yada, K.; Osaka, A. Self-Ordering of Cell Configuration of Anodic Porous Alumina with Large-Size Pores in Phosphoric Acid Solution. *Jpn. J. Appl. Phys.* **1998,** *37*, L1340–L1342.
40. Ripoll, C.; Müller, G.; Selegnye, E. Weak-Base Polyelectrolytes. 2. Determination of p*K*a of Poly-(2-vinylpyridine) and Activity Coefficients of Small Ions of Solution—Discussion and Conclusion. *Eur. Polym. J.* **1971,** *7*, 1393–1409.
41. Chu, B. Structure and Dynamics of Block Copolymer Colloids. *Langmuir* **1996,** *11*, 414–421.
42. Moffitt, M.; Khougaz, K.; Eisenberg, A. Micellization of Ionic Block Copolymers. *Acc. Chem. Res.* **1996,** *29*, 95–102.
43. Flory, P. J. Statistical Mechanics of Swelling of Network Structures. *J. Chem. Phys.* **1950,** *18*, 108–111.
44. Flory, P. J. The Configuration of Real Polymer Chains. *J. Chem. Phys.* **1949,** *17*, 303–310.
45. Pincus, P. Excluded Volume Effects and Stretched Polymer Chains. *Macromolecules* **1976,** *9*, 386–388.
46. Ma, M. L.; Krikorian, V.; Yu, J. H.; Thomas, E. L.; Rutledge, G. C. Electrospun Polymer Nanofibers with Internal Periodic Structure Obtained by Microphase Separation of Cylindrically Confined Block Copolymers. *Nano Lett.* **2006,** *6*, 2969–2972.
47. Kalra, V.; Mendez, S.; Lee, J. H.; Nguyen, H.; Marquez, M.; Joo, Y. L. Confined Assembly in Coaxially Electrospun Block-Copolymer Fibers. *Adv. Mater.* **2006,** *18*, 3299–3303.
48. Ruotsalainen, T.; Turku, J.; Heikkila, P.; Ruokolainen, J.; Nykanen, A.; Laitinen, T.; Torkkeli, M.; Serimaa, R.; ten Brinke, G.; Harlin, A.; Ikkala, O. Towards Internal Structuring of Electrospun Fibers by Hierarchical Self-Assembly of Polymeric Comb-Shaped Supramolecules. *Adv. Mater.* **2005,** *17*, 1048–1052.